Adsorption (2014) 20:5–20
DOI 10.1007/s10450-013-9544-1

Linking pore diffusivity with macropore structure of zeolite adsorbents. Part I: three dimensional structural representation combining scanning electron microscopy with stochastic reconstruction methods

E. S. Kikkinides · M. G. Politis

Received: 14 December 2012 / Accepted: 23 March 2013 / Published online: 31 March 2013

Abstract In the present study we have employed advanced experimental and computational methods to characterize the structure of a binderless zeolite adsorbent with improved mass transfer characteristics. Hence, we have used standard and hybrid simulated annealing (SA) methods to stochastically reconstruct in three dimensions the adsorbent structure, by matching low order correlations, namely porosity and two point correlation function. These correlations are measured on two dimensional images obtained by Back-Scattered SEM micrographs taken on different samples of the adsorbent. In the standard SA method we have started from a purely random structure, while in the hybrid method we have started from a uniformly consolidated random sphere pack made by the Lubachevsky–Stillinger algorithm. It is found that the hybrid method preserves, besides low order correlations, pore and mass chord length distribution functions, which contain information on higher order correlations, while the standard SA method matches only low order correlations. This is because in the hybrid process we have initiated the SA algorithm starting from a structure that contains structural information of the sintered zeolite powder, in the form of a consolidated random sphere pack with the porosity of the final structure. Evidently, diffusion studies will enable us to further evaluate the structures developed by each method, as will be explored in a subsequent study.

E. S. Kikkinides · M. G. Politis
Department of Mechanical Engineering, University of Western Macedonia, Bakola & Sialvera Str., 50100 Kozani, Greece

E. S. Kikkinides (✉) · M. G. Politis
Chemical Process and Energy Resources Institute (CPERI), Centre for Research and Technology Hellas (CERTH), P.O. Box 60361, 57001 Thessaloniki, Greece
e-mail: kikki@cperi.certh.gr

Keywords Stochastic reconstruction · Simulated annealing · Zeolite adsorbents · Scanning electron microscopy · Image analysis

1 Introduction

Pressure or vacuum swing adsorption (PSA, VSA) has become an established gas separation technology. There are several important commercial applications of PSA including, air separation, hydrogen recovery from steam methane reformer and air drying (Ruthven 2000; Sircar 2001, 2002). Improvement of a PSA process efficiency can be achieved primarily by improving the adsorbent material and the process cycles and to a lower degree by advancing the design of the adsorber bed. Details on the basic principles of gas separations by adsorption processes can be found in classic textbooks (Ruthven 1984; Yang 1987; Ruthven and Farooq 1994; Do 1998).

Since the invention of synthetic zeolites in 1959, innovations in the development of adsorbents and adsorption process cycles have made adsorption a key separations tool in the chemical, petrochemical and pharmaceutical industries. The past three decades have shown an explosion in the development of new nanoporous adsorbents. These materials have been fabricated to either improve the performance of specific separations or to treat separations that could not be performed using existing adsorbents. An excellent review on the fundamental factors controlling the design of adsorbents for various applications is provided by Yang (2003). In that review the main emphasis is on the equilibrium adsorption characteristics, normally described in the form of adsorption isotherms.

Nevertheless, adsorption based separations are influenced by both equilibrium and kinetic effects. Even in equilibrium-

driven separations the kinetic factor can be often very important in improving the overall process performance. Ackley and Leavitt (2002) have demonstrated that unexpectedly high gains in PSA process performance can be achieved for the case of air separation for O_2 recovery, using LiX zeolite adsorbent in the form of beads, when the mass transfer rate is increased. The main parameter in the work of Ackley and Leavitt (2002) that controls mass transfer, is the mass transfer coefficient for N_2, k_{N_2}, which has units of inverse time. Evidently, the higher the value of k_{N_2}, the higher is the mass transfer rate. This parameter depends on N_2 pore diffusivity, particle (bead) size and porosity (Todd and Webley 2002). More specifically, k_{N_2}, increases with particle porosity, however there is a trade-off between adsorbent strength and mass transport resistance resulting in typical particle porosity values between 30 and 40 %. Reducing the adsorbent particle size can also increase the value of $k_{N_2}$and reduce accordingly the length of mass transfer zones. However, at the same time, smaller particles will increase pressure drop along the adsorber bed, unless its length is decreased appropriately (Wankat 1987). Furthermore, as the particles become smaller, they are more difficult to immobilize and retain in the adsorber, increasing the potential for fluidization (Ackley and Leavitt 2002). The net effect is an undesirable increase in energy consumption of the process. Thus, the only parameter that can be manipulated to increase the overall mass transfer rate of the adsorbent, without causingany negative side effect in the process, is pore diffusivity, which in general depends on both micropore (intra-crystalline diffusion) and macropore structural characteristics.

It is known from past studies that agglomerated samples of A- and X-type zeolites exhibit macropore diffusion control at ambient temperatures (Karger et al. 1981; Karger and Ruthven 1992; Ruthven and Xu 1993; Papadopoulos et al. 2007). Hence for the case of N_2 and O_2 diffusion through LiX zeolite agglomerates, intrinsic pore diffusivity is governed by gas diffusion in the macroporous structure, while intra-crystalline diffusion can be safely neglected. Thus the main goal in fabricating appropriate zeolite adsorbents for air separation is to design macropore networks with increased diffusion characteristics while maintaining adequate strength with reasonable porosity limits of the agglomerated adsorbent particle. More specifically, Ackley and Leavitt (2002) have proposed a pore diffusivity for N_2, $D_{p,N_2} \geq 3.5 \times 10^{-6}$ m^2/s, when measured at a pressure of 1.5 bar and at a temperature of 300 K, which can lead to significant impact upon process performance, for cycle times less than about 1 min. For shorter cycle times of the order of 15 s or less, even higher diffusivity values must be achieved (Ackley and Leavitt 2002; Ackley and Zhong 2003).

Commercial zeolite adsorbents are made in the form of macroporous beads of suitable dimensions, porosity and mechanical strength. There are various agglomeration methods including extrusion, granulation and combined processes (Breck 1984; Dukić-Ott et al. 2009). In general a binder is added to help cement the zeolite crystallites together and achieve adequate mechanical strength. The binder, which is often made of clay, has negligibly small capacity for gas adsorption and amounts to 10–20 % in the final product (Jasra et al. 2003).

Previous research has shown that the distribution of the binder in the agglomerated zeolite adsorbent is a random process, with the majority of the binder particles being in contact with the zeolite crystallites or with other binder particles (Chao and Pontonio 2002). For the case of clay-made binders the fine particles of clay form a sponge-like structure, which either bridges the gap between zeolite crystallites or simply coats them, but at the same time it blocks the macropores and increases mass transfer resistance of the agglomerated adsorbent. Binderless adsorbents can be made, using "zeolitizable clays", including kaolin or kaolin-type clays, as binders and subsequent caustic digestion to convert the clay to zeolite after bonding (Chao and Pontonio 2002). Such adsorbents have been reported to have structural and mass transfer characteristics that meet the targets set above (Chao and Pontonio 2002; Ackley et al. 2003).

Unfortunately it has been well realized that the manufacture of agglomerated zeolite adsorbents, with or without binder, has been much of an art as a science and much manufacturing knowledge has been obtained from a series of experimental programs, followed by trial and error methodologies. As a result, most efforts made to improve mass transfer characteristics in the inter-crystallite macroporous structure, have been based on pore morphology description through mercury (Hg) porosimetry characterization.

Hg porosimetry is by far the most popular method for characterizing porous materials with pores in the range of $\sim$100 μm down to $\sim$0.003 μm (Lowell and Shields 1991; Leon y Leon 1998, Rouquerol et al. 2012). Compared to alternative characterization methods such as gas sorption, Hg porosimetry covers a much wider pore size range, while it is based on a simpler physicochemical principle (the Washburn equation) and it is much faster in operation. Nevertheless, Hg porosimetry has some important limitations that must be taken into account when analyzing the structure of porous materials, particularly when there is no additional/complementary information from other characterization techniques, such as microscopy, tomography, small and very small angle scattering, etc. In particular, the method is based upon the assumption of straight cylindrical pore geometry and can lead to misleading structural

information when pores are not cylindrical in shape, or when large pore volumes are connected by narrow pores (pore shadowing or ink-bottle effect) in conjunction with limited accessibility or connectivity issues (Leon y Leon 1998). Thus, despite efforts to correlate structural information provided by Hg-porosimetry with pore diffusivity or tortuosity (Carniglia 1986), it is generally evident that this method cannot provide a solid and robust link between pore structure and diffusivity.

It has been long realized that the direct interpretation of experimental flow or diffusion data from real porous materials in relation to the underlying microstructure is cumbersome due to the geometrical complexity of the porous matrix. Although considerable progress has been made in the efficient representation of the internal architecture of porous media using pore networks (see for example, Burganos and Sotirchos 1987; Sahimi et al. 1990; Hollewand and Gladden 1992; Zhang and Seaton 1992, and references cited therein) there exists a strong need for a direct quantitative geometric description of the complex porous structure. The relentless advances in computational speed and powerful new methodologies have provided the basis for a reliable determination of macroscopic transport properties (Adler 1992; Torquato 2002).

More particularly, over the last three decades (with more progress over the last 15 years) there have been various studies that propose advanced mathematical methods that can produce off-lattice or on-lattice (digital) 3D replicas of the actual porous structures. These replicas preserve the basic structural information of the original materials and predict pore diffusivities with very good accuracy (Levitz 1998; Kainourgiakis et al. 1999, 2002; Kikkinides et al. 2004; Čapek et al. 2011), without the need to resort to any adjustable parameter as it normally done in pore network models. The aforementioned mathematical methods are classified as process-based, and statistical reconstruction methods. Attempts have been also made for the direct 3D computer reconstruction of detailed pore structure data obtained by serial sectioning of pore casts or computed tomography imaging (e.g. synchrotron X-ray or nuclear magnetic resonance). However, serial sectioning is laborious, time-consuming and operator-depended, while tomographic imaging is still limited to micron-range resolution, high costs and equipment accessibility. Process based methods account for the major physical processes underlying the formation of certain porous structure. Well known examples include sedimentary rock and sandstone representation by modeling different rock-forming geologic processes (Roberts and Schwartz 1985; Øren and Bakke 2002). Process-based reconstruction methods, although more sound from a physical point of view, suffer frequently from severe computational requirements and are limited to the specific material considered. An attractive alternative is offered by the statistical methods in terms of a stochastic simulation of porous media in 3-D utilizing statistical information obtained from relatively few 2-D images of thin sections. The basic principle is that both real and model structures should have the same basic statistical content, which is represented by one and two-point correlation functions and is used as input for the creation of the simulated structures under the assumption of statistical homogeneity (Adler 1992; Torquato 2002). In this case, information on the aforementioned statistical properties of the materials is obtained directly from serial tomography, SEM/TEM micrographs, fluorescence confocal optical microscopy FCOM, Bonilla et al. 2001), and indirectly, by small or very small angle scattering (SAS) data, depending on the length-scales involved in the porous structure that is characterized (Levitz and Tchoubar 1992).

More recently, hybrid reconstruction methods have been proposed in an effort to link additional structural information or/and improve computational requirements in the reconstruction process (Talukdar et al. 2002a; Politis et al. 2008). The advantage of hybrid methods is that they can increase the computational speed significantly. Furthermore, incorporation of a porous structure made by a process-based method, as an initial condition to the stochastic reconstruction method, with additional manipulation of the latter process, allows us to achieve agreement of higher order correlations or other structural properties implicitly. Obviously this can only be true if we have some previous knowledge of the history of structural formation of the porous material. For example if we examine a material that we know that has originally started from the treatment of spherical particles then an initial configuration of a random sphere pack (RSP) is expected to improve the accuracy of the final structure (Politis et al. 2008).

In the present study, we report on the three-dimensional representation of the structure of a binderless zeolite adsorbent that have been previously developed and meets the targets of N_2 pore diffusivity, $D_{p,N_2} \geq 3.5 \times 10^{-6}$ m^2/s, at a pressure of 1.5 bar and at a temperature of 300 K. In part I of this publication series, stochastic reconstruction methods are applied to generate three-dimensional porous structures that match the basic statistical properties measured on two-dimensional SEM images of the actual materials. We employ the simulated annealing (SA) technique starting either from a purely random structure or from a RSP (hybrid method). Differences in the porous structure given by the use of different reconstruction methods (SA and hybrid) are evaluated based on the differences on measured chord length distribution functions, that account for higher order correlations in the porous matrix. In Part II, we further evaluate each developed structure by simulating N_2 diffusion using a step by step Monte Carlo random walk process and Hg-intrusion porosimetry using a purely morphological model. The

resulting N_2 pore diffusivities and Hg-intrusion curves for each structure are compared with each other and with experiments, in an attempt to show how pore diffusion and Hg-intrusion are affected by structural differences and which reconstruction method is more suitable in the case of the zeolite adsorbent examined in the present study. Evidently, the ultimate goal of such a study will be to identify the main structural characteristics that control the mass transfer rate in the zeolite adsorbent. It is expected that improvement of these selected key structural parameters will enhance mass transfer rate in the adsorbent and hence process performance characteristics in a PSA/VSA operation.

2 Experiments and methods

The binderless LiX zeolite adsorbent employed in the present study has been fabricated by Praxair, Inc. in the form of spherical beads of average particle size of 1.25 mm (Chao and Pontonio 2002; Ackley et al. 2003). The macroporous structure has been characterized using scanning electron microscopy (SEM) and Hg porosimetry. The adsorbent has porosity $\varepsilon = 0.379$ as measured by Hg porosimetry and N_2 pore diffusivity $D_{p,N_2} = 4.2 \times 10^{-6}$ m^2/s at a pressure of 1.5 bar and a temperature of 300 K, as determined by a standard methodology that combines breakthrough experiments with detailed modeling (Ackley et al. 2003; Todd and Webley 2005). More details on the synthesis and fabrication process of this material are provided in the patents of Chao and Pontonio (2002) and Ackley et al. (2003).

2.1 SEM analysis

The imaging of the beads has been performed using a SEM instrument of diamond-paste polished sections and employing a back-scattered electron (BSE) mode (Chao and Pontonio 2002). In the BSE mode, variations in the average atomic number of the material correspond to variations in the gray-scale level of the image. Prior to polishing, the samples are impregnated with an epoxy resin, out-gassed under vacuum, to enhance contrast and preserve the structural integrity of the material. Next, the samples are ground to a smooth flat surface using silicon carbide papers or cut using a diamond wheel. Finally, a non-thermal oxygen plasma is used to eliminate the surface layer of epoxy in order to expose the adsorbent material, and in so doing, enhance the quality of the resulting SEM images. Prior to image acquisition, the polished surface of the sample is spritzed with gold to increase the conductivity and prevent charging phenomena that similarly reduce the SEM image quality. The lower average molecular weight of the resin results in pores to be seen as dark objects in a brighter background. A sufficient number of images providing information about the composition of polished sections have been obtained for the statistical characterization of the porous structure. Images are digitized and saved as unsigned 8-bit integer with a gray-scale intensity range from 0 to 255, with a typical spatial resolution of 1,280 × 960 pixels and a magnification of 4,500×. The correct choice of pixel size and magnification is paramount for capturing the micro-structural characteristics of the porous matrix.

2.2 Image processing and analysis

Even if every care has been taken to avoid introducing noise or artifacts, SEM/BSE image acquisition can never be perfect (Echlin 2009). Although the quality of the SEM/BSE images cannot be enhanced by post-processing it can certainly be improved by appropriate image analysis methods. Some noise appears and it is necessary to remove or reduce it. Visual inspection of SEM image samples revealed areas that virtually no resin impregnated the pore structure. The resulting contrast is particularly poor and background solids cannot be clearly distinguished from the surface as can be seen in Fig. 1. Furthermore, some zeolite crystals located close to the external surface appeared to be artificially fragmented or sheared.

In order to avoid this undesirable effect and also be consistent with the constrains of statistical isotropy and homogeneity, it was deemed necessary to develop a consistent methodology for producing the purely 2D binary equivalents of the SEM micrographs (Gonzalez and Woods

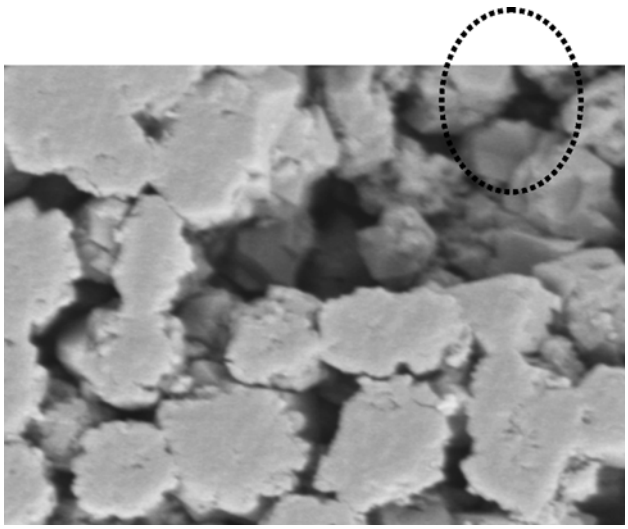

Fig. 1 SEM micrograph of bead sample-1. Background solid is clearly visible in the *upper right corner*. Classifying the pixels in the dashed circle area can be problematic: contrast between surface and background solid is poor

2008). This methodology involves anisotropic diffusion filtering and adaptive thresholding of the images (Gonzalez et al. 2009; Russ 2011).

SEM image resolution is 1,280 × 960 pixels with a resolution of 10 μm/450 pixel (0.0222 μm/pixel). The higher the resolution, the more pixel elements are used for each unit length. This enhances the available spatial information and overall accuracy of the macroscopic property calculated in the reconstructed domain. Any detailed spatial information below 0.0222 μm is lost. This fact must be also taken into account when comparing the porosity calculated from the SEM images with experimental results from Hg porosimetry. Spatial resolution is very important when deciding what images to use and it is a rule of thumb to have a least 3–5 characteristic unit lengths per domain at the highest possible resolution, for statistically meaningful structural and transport calculations (Torquato 2002). These characteristic lengths can be directly related to the correlation length of each structure, which is roughly the distance beyond which the two-point auto-correlation function of the structure remains equal to zero. After scrutinizing the available samples using the aforementioned criteria, three of them (sample-1, sample-2 and sample-3) have been selected as most appropriate for analysis.

2.2.1 *Choice of the thresholding method*

Thresholding involves separating an image into regions that in the case of a two-phase porous medium are only two: solid and void (pore). Usually black is set to a grey-scale value of (0) and white to (255). In this work, solid phase is shown as white (bright) and pore space as black (dark). Thresholding creates binary images from grey-level ones by turning all pixels below some threshold to zero and all pixels about that threshold to one. Mathematically, if $g(x, y)$ is a thresholded version of $f(x, y)$ at some global threshold T_h, then:

$$g(x,y) = \begin{cases} 1 & \text{if} \quad f(x,y) \le T_h(x,y) \\ 0 & \text{if} \quad f(x,y) \ge T_h(x,y) \end{cases} \tag{1}$$

The problem with global thresholding, is that it fails when the contrast is poor, like different illumination intensity in a picture. For our case this means that classifying pixels around the solid-pore interface becomes difficult because of the little contrast with the background solid. In a reference-case scenario, the histogram would be distinctively bimodal, showing a pronounced ‘valley’ between the two intensity peaks. In such case, selecting a global threshold is straight-forward and less error-prone; simply select some value between the two peaks by using any established global thresholding algorithm (Russ 2011).

All digital image processing and analysis was performed using the public domain software ImageJ, developed by W. Rasband (Collins 2007; Girish and Vijayalakshmi 2004; Schneider et al. 2012) at the National Institute of Health, USA and appropriate plug-ins, supplemented by an in-house Matlab code.

Next, we investigated the effect of the threshold value in the original grayscale SEM image on the porosity of the resulting binary image. The resulting porosity-threshold diagram is shown in Fig. 2. The sigmoidal shape of the curve indicates a strong non-linear relation, especially around the percolation-like transition in the region of the mode value (146). The unimodal shape makes setting a global threshold much more error-prone.

It should be noted that another way to overcome the poor results of automated global thresholding would be to manually adjust the threshold and edit (retouch) the images on case-by-case basis. The drawback is the lack of reproducibility and that it is overly operator-dependant. This makes comparisons between samples and sometimes even within the images of one sample questionable. Because comparisons are important in this study, we have pursued an automated (and algorithmic) approach. After reviewing the literature (Baveye et al. 2010; Sezgin and Sankur 2004; Tarquis et al. 2008) and experimenting with different algorithms implemented as ImageJ plug-ins (Landini 2011) the adaptive thresholding approach was chosen. The criteria used to decide on the algorithm are: (1) the porosity must match, as close as possible, given the resolution limitations described above, with what was expected from Hg intrusion porosimetry results for the samples and (2) the visual comparisons of the morphology match, especially the shape of the solid ‘coastline’ in the binary image.

Following the suggestions of Manay and Yezzi (2003) that information about the best local threshold is expected to be found near image edges (transitions between foreground and background) on a smoothed version of the image, we decided to introduce a pre-processing step, the anisotropic diffusion filtering.

Adaptive methods (Russ 2011) are based on local information (e.g., local window histograms) by defining an $N \times M$ pixel window (sub-image) around each pixel. A threshold is computed based on that local view of the image using any method available (such as a thresholding algorithm or statically set by the user). This allows the threshold to adapt (be adjusted) to each pixel location and thus use meaningful spatial information to distinguish between the background ‘shadow’ solid and the ones in the surface. If a global threshold is used then the classification of the pixels in the pores outline (edge) are misclassified as pore or solid depending on the value of the threshold (or method) used. In the particular ImageJ implementation used in our analysis (Landini 2011; Shapiro and Stockman

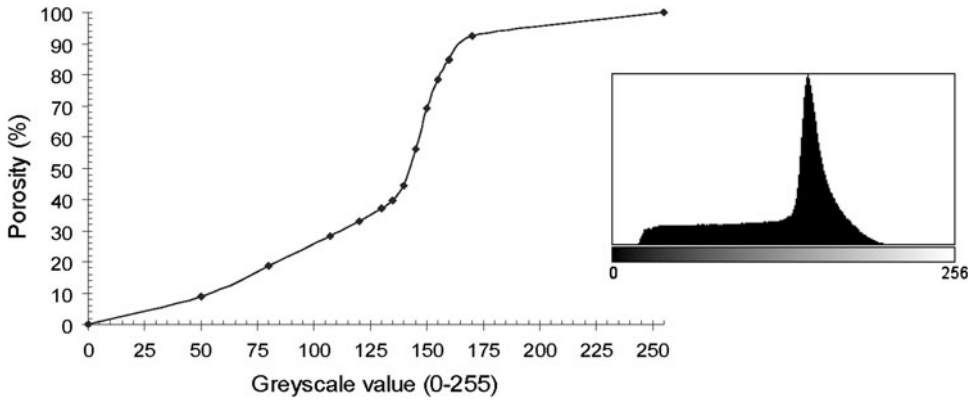

Fig. 2 Influence of threshold selection on porosity (sample-1). The corresponding histogram is shown on the *right*

2001) we had to specify the window size in pixels and a weighting constant.

2.2.2 *Anisotropic diffusion*

Anisotropic diffusion filtering is an image 'smoothing' step that levels the solid phase pixels while preserving the edge morphology. Other smoothing operators applied, like median (or mean) filtering were over-smoothing, significantly altering the porosity of the resulting binarized structure. This processing step proved useful since the greyscale values on either side of a sharp edge form very poor thresholds when compared to the "average" greyscale value encountered in the middle of a smoothed edge, a fact that is exacerbated by poor contrast, as in the case of processed samples.

Application of anisotropic diffusion results in the production of a Gaussian smoothed image, which is the solution to the heat equation, with a variable conductance term to limit smoothing at edges. The filter implementation used was that of Tschumperle and Deriche (2005) as it is included in the ImageJ software. The conductance term is a function of the gradient magnitude of the image at each point. This filter requires 3 parameters: the number of iterations to be performed, the time step, and the conductance parameter used in the computation of the level set evolution. The values used in all cases were 20 iterations and a dimensionless time step of 0.2. The conductance parameter is specified by two coefficients with default values, left unchanged, $a_1 = 0.5$ (diffusion limiter along minimal variations) and $a_2 = 0.9$ (diffusion limiter along maximal variations). Once nonlinear anisotropic diffusion attenuates the intensity of noise artifacts, especially in the vicinity of particle edges, solid-void segmentation is obtained by an adaptive local threshold algorithm, as described above. The result is better contrast and thus less misclassifications, especially less isolated pore pixels on the material (processing 'noise').

3 Computational methods

3.1 Microscopic characterization of porous structure

3.1.1 *Basic assumptions and definitions*

A porous material can be defined as a binary medium that contains two phases: the solid phase and the pore space. Accordingly it can be described rigorously by the *phase function* $Z(\mathrm{x})$, which is defined as follows (Adler 1992; Torquato 2002):

$$Z(\mathbf{x}) = \begin{cases} 1 & \text{if } \mathbf{x} \text{ belongs to the pore space} \\ 0 & \text{otherwise} \end{cases} \quad (2)$$

The phase function can be used to define several important properties that can statistically describe a porous medium.

3.1.2 *Spatial correlation functions*

The n-point correlation function is a measure of the probability of finding n-points (in a specified geometrical arrangement) all lying in the region of space occupied by one constituent of a two-phase material. Following the definition of the phase function $Z(\mathbf{x})$, it is straightforward to recognize that the probability of finding a point with position $\mathbf{x}$ in the pore space is identical to the value of its phase function, $Z(\mathbf{x})$ or simply: $P(Z(\mathbf{x}) = 1) = Z(\mathbf{x})$. Then the general definition of the n-point correlation function, (also defined as the [n-1]-order moment of the phase function) is:

$$S_n(\mathbf{x}_1, \mathbf{x}_2, \ldots, \mathbf{x}_n) = \left\langle \prod_{k=1,n} Z(\mathbf{x}_k) Z(\mathbf{x} + \mathbf{u}_k) \right\rangle \quad (3)$$

For example the 1-point correlation function, or zero order moment, is the probability that any point lies in pore space. Then it follows that the 1-point correlation function is by definition equal to the porosity:

$$\varepsilon = \langle Z(\mathbf{x}) \rangle \tag{4}$$

Accordingly the 2-point correlation function, or first order moment, is the probability that two points a specified distance **u** apart, are both in the pore space of the material:

$$S_2(\mathbf{u}) = \langle Z(\mathbf{x}) \cdot Z(\mathbf{x}+\mathbf{u}) \rangle \tag{5}$$

For an isotropic medium, $S_2(\mathbf{u})$ becomes one-dimensional as it is only a function of $u = |\mathbf{u}|$ The two point correlation function can be obtained by randomly tossing line segments of length u and counting the number of times the end points fall in the void (or solid) phase. Alternative, more rigorous ways of measuring $S_2(\mathbf{u})$ in digitized media are given by Berryman (1985).

It is often preferable (Adler 1992; Torquato 2002) to work with the 2-point auto-correlation function $R_z(\mathbf{u})$ which is a normalized version of $S_2(\mathbf{u})$:

$$R_Z(\mathbf{u}) = \frac{\langle (Z(\mathbf{x}) - \varepsilon) \cdot (Z(\mathbf{x}+\mathbf{u}) - \varepsilon) \rangle}{\varepsilon - \varepsilon^2} \tag{6}$$

Note that if we reverse the phase function in order to calculate the n-point correlation functions for the solid phase we observe that $R_z(\mathbf{u})$ remains unaltered (Torquato 2002).

The specific surface area of the material, S_v, can be determined from the slope of the autocorrelation function using the following equation (Adler 1992; Torquato 2002):

$$S_v = -4S_2'(0) = -4\varepsilon(1-\varepsilon)R_Z'(0) \tag{7}$$

where $S_2'(0)$, $R_Z'(0)$ are the slopes of $S_2(u)$ and $R_z(u)$, respectively, at $u = 0$. Thus, the 2-point correlation function contains useful information on the interface area per unit volume of the material. Note that the above equation holds for any continuous material. For a digitized medium $S_v = -2dS_2'(0)$, d being the dimensionality of the medium (Yeong and Torquato 1998a).

A random medium is said to be statistically homogeneous if the n-point correlation functions are translational invariant (Torquato 2002). This means that all regions of space are statistically similar and it further suggests the ergodic hypothesis, usually met in stochastic processes (Torquato 2002), according to which, the result of averaging over all realizations of space is equivalent to averaging over the volume of one realization in the infinite volume limit (i.e. volume average is equivalent to ensemble average).

Ideally, a representative reconstruction of a porous medium in three dimensions should have the same correlation properties as those measured on a single two-dimensional section, expressed properly by the various moments of the phase function. In practice, matching of the first-two moments, that is, porosity and two point correlation function, has been customarily pursued (Adler 1992; Torquato 2002). This simplification is often shown to be invalid as one can find examples of porous media exhibiting quite different morphological properties while sharing the same 2-point correlation function (Roberts 1997; Kainourgiakis et al. 2000; Talukdar et al. 2002b; Čapek et al. 2009; Jiao et al. 2010). In other words while reproduction of the porosity and two-point correlation function is always necessary, it is not always sufficient for a faithful representation of the porous microstructure. In this case one should try to match multi-point correlation functions. Such an approach is however, quite tedious making the whole exercise difficult to handle. For this reason several other statistical descriptors have been defined in an effort to improve the accuracy of the developed structure at lower computational requirements (Torquato 2002; Jiao et al. 2009, 2010).

3.1.3 *Chord length distribution function*

The chord-length probability density function or chord-length distribution function, $p_i(x)$, is directly related to the probability $p_i(x)dx$, that a chord of length between x and $x + dx$, lies in phase i of a statistically isotropic medium. When applied to porous media characterization, chord length distribution functions are distinguished as pore and mass chord length distribution functions when measured at the void and solid phase of the material, respectively.

Knowledge of the chord-length density function is of basic importance in transport problems involving discrete free paths and thus has application in Knudsen diffusion and radiative transport in porous media (Torquato 2002). The mean chord length for phase i, l_i, is defined by

$$l_i = \int_0^\infty x p_i(x) dx \quad , i = p, m \tag{8}$$

It can be shown that the mean pore chord length, $\langle l_p \rangle$ is equal to the hydraulic pore diameter of a porous material, d_h, defined by the well known expression:

$$d_h = \frac{4\varepsilon}{S_v} \tag{9}$$

where ε is the porosity and S_v the specific surface area of the material, already defined above. Thus information on pore chord length can be related to the average pore size of the material.

Contrary to the two point auto-correlation function, the chord-length distribution function is not the same in the void and solid phase of a porous material. It has been shown before that the chord length distribution function contains information from higher order moments of the phase function and can be thus used as an alternative, computationally less expensive measure of these moments (Torquato 2002). Note that another interesting and useful

statistical descriptor that accounts for higher order correlations is the lineal-path function L_i, which gives the probability that a line segment of length x lies wholly in phase i when randomly thrown into the sample. It can be seen that lineal path functions are related to chord length distribution functions via relatively simple mathematical expressions (Torquato 2002).

3.2 Three dimensional representation of the porous structures

3.2.1 Stochastic reconstruction

Statistical methods are based on the stochastic simulation of porous media in 3-D utilizing statistical information obtained from relatively few 2-D images of thin sections. The basic underlying principle is that both the real and the model structures should have identical statistical properties, such as average porosity and autocorrelation function which are used as input for the creation of the simulated structures under the assumption of statistical homogeneity (Adler 1992). Statistical or stochastic reconstruction methods have been proposed for the representation of different classes of porous media from hydrocarbon reservoirs to porous filters and down to nano-structured membranes. Depending on the characteristic length scale of each class of material a different degree of resolution is required in each case. Therefore information on the aforementioned statistical properties of the materials is obtained directly from SEM (resolution of the order of μm) or TEM images (resolution of the order of nm) or indirectly by SAS data. In the latter case resolution varies from nm (SANS-SAXS) to μm (very small angle neutron scattering).

There have been various statistical reconstruction methods proposed in the open literature. The two most popular ones are Gaussian random fields (GRF) (Adler 1992) and SA (Yeong and Torquato 1998a, b). The SA method is in general more powerful than the GRF method as it can include more statistical information and produce more accurate representations of the pore structure. Moreover, it can be easily adapted to be employed in hybrid reconstruction process. However, it requires significant computational power due to the large number of operations required at each step, and the slow convergence to the optimal structures. In the present study we will focus on the SA method, whose main features are described below.

3.2.2 The SA method

SA was originally proposed in 1983 by Kirkpatrick and coworkers (Kirkpatrick et al. 1983), who considered the use of the Metropolis algorithm to solve some of the typical combinatorial problems appearing in the field of circuit design. To achieve this, they established an analogy between the annealing process in solids, the behavior of systems with many degrees of freedom in thermal equilibrium at a finite temperature and the optimization problem of finding the global minimum of a multi-parameter objective function. Yeong and Torquato (1998a, b) have adapted the SA method to simulate the structure of porous materials.

In the pertinent method, a randomly generated perturbation of the current configuration of the system under study is applied so that a trial configuration is obtained. Let E_c and E_t denote the energy level of the current and trial configurations, respectively. If $E_c \geq E_t$, then a lower energy level has been reached, the trial configuration is unconditionally accepted, and becomes the current configuration. On the other hand, if $E_c < E_t$ then the trial configuration is accepted with a probability given by:

$$P(\Delta E) = \exp\left(-\frac{\Delta E}{k_B T}\right) \tag{10}$$

where $\Delta E = E_t - E_c$, k_B is Boltzmann constant and T is the temperature (or an arbitrary analog of it, used only to symbolically represent the degree of randomness in the spatial distribution of the system phases). This step prevents the system from being trapped in a local lowest-energy state. After a sufficient number of iterations, the system approaches equilibrium, where the free energy reaches its minimum value. By gradually decreasing T and repeating the simulation process (using every time as initial configuration the one found as equilibrium state for the previous T value), new lower energy levels become achievable. The process is considered complete when despite the change in T, the number fraction of accepted changes in different configurations becomes lower than a pre-specified value (e.g. 1×10^{-4}).

The above procedure is easily adopted in our case as follows:

We start from an initial random distribution of the phase function in space, ensuring that the porosity of the structure is equal to the targeted one. The initial temperature is $T = 1 \times 10^{-3}$, in accord with previous studies (Cule and Torquato 1999; Politis et al. 2008).

The next step is to define the Energy, E, of our system. In the case of the stochastic reconstruction of a porous medium, E is the sum of squared differences between experimental correlation functions obtained from the SEM micrographs, and those calculated from the 3D generated structure.

$$E = \sum_i \sum_j \left[S_i(u_j) - S_i^{\exp}(u_j)\right]^2 \tag{11}$$

where index i, corresponds to the degree of the correlation function, and index j, corresponds to the digitized distance u.

If only the two-point correlation function interests us, then $i = 2$ and the first summation is dropped out from Eq. (11). Note that in the above algorithm the one-point correlation function (porosity) is always identical to the targeted one by construction (fixed system porosity).

The SA algorithm in this case is applied as follows (Yeong and Torquato 1998a, b):

1. Starting from a given structure, we calculate the initial Energy, E_c from Eq. (11).
2. A trial state is considered by interchanging (swapping) two arbitrarily selected pixels of different phases. This way the initial porosity of the structure is always preserved. Accordingly the energy of the trial state E_t is determined again through Eq. (11).
3. If $E_c \geq E_t$, the trial configuration is unconditionally accepted, and becomes the current configuration. On the other hand, if $E_c < E_t$ then the trial configuration is accepted with a probability given by Eq. (10).
4. Steps 2, 3 are repeated until N_r Monte Carlo moves are accepted at the same temperature T, where $N_r = \lambda_{MC} N_x N_y N_z$. Parameters N_x, N_y and N_z, denote the size of the reconstructed replica (in pixels) in the x, y and z direction, respectively, while parameter $\lambda_{MC} = 10$, in accord with previous studies (Cule and Torquato 1999; Politis et al. 2008).
5. We decrease temperature by a very slow rate using an appropriate cooling schedule of the form $T_k/T = \lambda^k$, where k is the iteration index and λ is the annealing rate constant, $\lambda = 0.9$, in accord with previous studies (Cule and Torquato 1999; Politis et al. 2008) and we repeat steps 2–4.

The process is terminated when the number fraction of accepted changes in different configurations becomes lower than a pre-specified value (e.g. 1×10^{-4}) or when the temperature reaches zero (in practice a very low value e.g. 1×10^{-20}).

3.2.3 *Hybrid reconstruction*

In the typical SA method we start from a completely random initial distribution of the phase function in space. Alternatively we can start from an initial configuration provided by the output of a process-based method. It is known that in the manufacturing process of LiX zeolite adsorbents the starting materials are powders consisting of particles that can be considered as spherical (to a first degree of approximation) and have a quite narrow particle size distribution. Hence, in the present study, we employ a process-made method to produce mono-sized random spherical packs. The developed structures are subsequently consolidated to the desired porosity as measured on SEM micrographs and/or provided by Hg porosimetry. More particularly, in the present study we have employed the Lubachevsky–Stillinger (L–S) compression algorithm (Lubachevsky and Stillinger 1990; Torquato et al. 2000) to produce spherical packs with porosity $\sim$40 %. This algorithm is essentially a non-equilibrium hard-sphere molecular dynamics simulator in which N spheres ($N \sim 300$ in the present study), placed inside a unit box, grow in size during the course of the simulation at a certain constant expansion rate, until a final state with diverging collision rate (or equivalently constant packing fraction) is reached. Once the initial conditions are fixed, the system evolves deterministically. Thus, any randomness in the packing generated with the L–S algorithm is derived from the initial conditions. This algorithm has a single parameter which represents the sphere growth rate, a, relative to the mean sphere speed (Lubachevsky and Stillinger 1990; Torquato et al. 2000). As the spheres grow larger, the collision frequency increases, and a maximum packing fraction is asymptotically approached. The L–S algorithm produces random, "jammed" sphere packs with porosities of the order of 36 %. Nevertheless, in the present study we terminated the algorithm when a porosity of 40 % was reached and subsequently inflated the spheres of the pack until the desired targeted porosity $\sim$32 % of the adsorbent is reached. Note that the developed algorithm can treat spheres from any given theoretical or experimental particle size distribution. Nevertheless, experiments using either laser diffraction techniques or SEM on the loose zeolite powders have revealed a very narrow particle size distribution that can be considered as mono-sized as has been confirmed from similar studies.

The resulting structure is used as an initial distribution in the SA algorithm. Note that in this case the initial temperature T, must be low enough so that parts of the initial structure can be preserved during the SA process. Previous and current studies (Politis et al. 2008) on a great variety of materials have suggested a value of $T = 1 \times 10^{-10}$ as a most suitable starting temperature in the hybrid process.

Note that in the present work, the termination porosity of the random pack is considered to be 40 % instead of 36 %, which is the porosity at which the spheres jam, for two reasons: (a) We wanted to compare the results of the present work with previous unpublished results obtained using a ballistic deposition algorithm that is known to generate only loose RSPs with porosities around 40–42 %. (b) The present work is part of a more general study, where a large number of porous adsorbents with porosities ranging from 28 and up to 40 %, has been characterized and reconstructed using the present methodology. Thus we wanted to develop an initial RSP structure with a porosity that is large enough to manage this wide porosity spectrum. Nevertheless, we have performed additional hybrid reconstruction studies starting

from jammed RSPs with porosities of ~36 %. The results are almost unaffected in terms of either structural or diffusion properties. We believe that the sphere inflation-consolidation step for either RSP structure employed to produce an initial structure with a porosity that is equal to the adsorbent porosity of 32 %, followed by the SA procedure, smoothens any original structural difference between the 36 % and the 40 % RSPs.

4 Results and discussion

4.1 Image processing results

The resulting binary images with their respective porosity values for the three different bead-samples are presented in Fig. 3. Notice that the porosity in each case is around 32–33 % and that the samples from the three different beads have structural resemblance indicating statistical homogeneity at the relevant scale. The difference between the porosity measured by SEM and that measured by Hg porosimetry can be largely attributed to the resolution limitations of the former method to sizes <0.0222 μm (in this study), which fail to account for pores with size that is smaller than this value (mainly mesopores). Furthermore Hg-porosimetry is measured over the whole bead and also on a large number of beads, so it can give a more representative value of porosity for the adsorbent bead. Nevertheless, the relative difference between SEM and Hg porosity is between 12 and 15 %, which is considered reasonable based on the important differences and limitations outlined above.

The visual resemblance among the three images is further illustrated and quantified when determining the respective two-point auto-correlation functions, $R_z(u)$, as a function of distance u, in Fig. 4. It is seen that the respective auto-correlation functions look quite similar for all three images with the first two showing almost identical properties. In the same figure we have plotted the average R_z which will be used together with the average porosity of 32.2 % as input for an averaged reconstructed domain.

4.2 Stochastic reconstruction

The reconstruction of the zeolite adsorbent has been performed using the SA methodology (standard and hybrid) described in the relevant section above. The pixel size used is 0.0444 μm, which is two times the minimum pixel size of the original SEM image. This pixel size corresponds to a value of $R_z \sim 0.88$ at the smallest possible distance within the structure, and gives a total sample size of 9.4 μm (for a 212^3 3D structure), which is of comparable size with the original 2D SEM image (28.4 × 20 μm^2). The two-point correlation function is matched with the SA method for up to 60 length steps of size 0.0444 μm, which correspond to a total distance of 2.66 μm, where all correlations have already become well extinct. Note the ratio of sample size over correlation length is around 5 or more, which ensures meaningful calculations of structural and transport properties (Adler 1992; Kainourgiakis et al. 2002; Torquato 2002).

We have performed both standard and hybrid SA methods on the three selected bead samples and on a fourth sample made with an averaged porosity and two point correlation function over the three samples. In the standard SA method we start from a purely random structure with porosity equal to that of the target one, as measured in the SEM micrograph, at a relatively high initial temperature, $T = 1\times10^{-3}$. In the hybrid method, we start from a monosized RSP made of 300 spheres, with a final porosity 40 %, produced by the L–S compression algorithm. Accordingly, we perform a consolidation of the RSP structure by inflating uniformly all spheres of the pack until the desired targeted porosity of the SEM image is reached. Typical snap-shots during the formation of the RSP are shown in Fig. 5. Furthermore, the consolidation of the RSP is illustrated in Fig. 6, where we compare two-dimensional sections cut from random and consolidated sphere packs, respectively. The latter structure, which we call RSP-CS, is used as a starting domain in the hybrid SA process with an initial temperature, $T = 1\times10^{-10}$.

In Fig. 7, we present typical 2D sections cut from 3D structures made with the standard and hybrid method during different stages of the SA process along with the history of energy minimization for each method. It is seen that during the standard SA method that starts from an initially random configuration, the energy of the system remains constant and equal to its initial value, corresponding to this random structure for a large number of counts. Then, at a value of around 100 counts it starts dropping and there we observe a transition from a random to a correlated structural formation, which is further refined and stabilized after about a total of 250 counts. The hybrid method, on the other hand, has a completely different behavior: Initially we start from a RSP-CS structure whose formation has been described above. We see that even at the beginning of this process the energy of the system is quite low, indicating the structural relevance of the initial configuration in this case. Then as the SA proceeds we observe how the structural characteristics are tuned up until the final structure is obtained with a very low final energy at a significantly lower number of counts (around 90).

Looking at Fig. 7, we observe distinct visual differences between the 2D-sections of the structures made by the two different reconstruction methods.

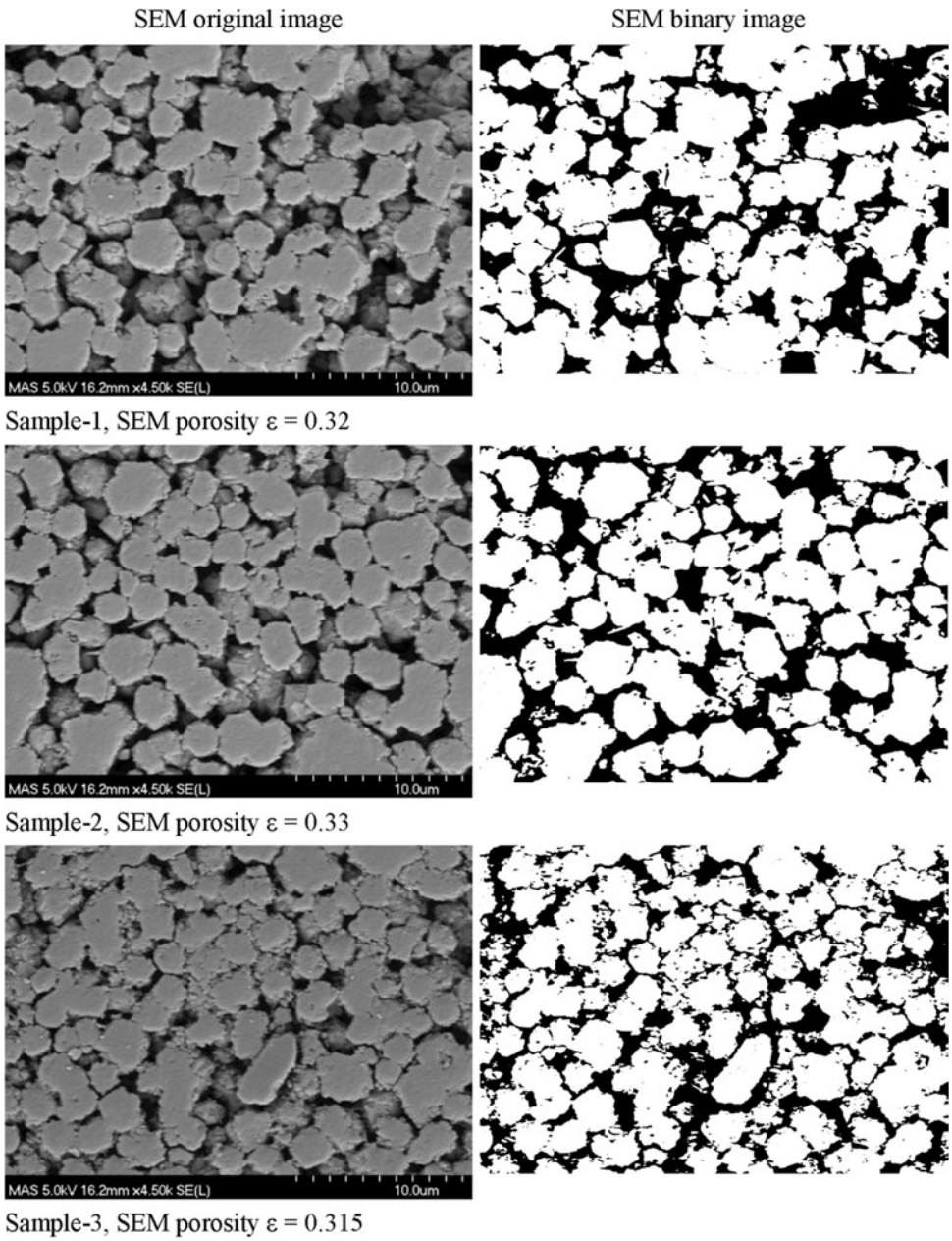

Fig. 3 Original (*left*) and binarized (*right*) domains of BSE/SEM micrographs. In the latter, *black color* corresponds to void and *white color* to solid phase, respectively

4.3 Structural characterization

To quantify the above visual observations we have calculated the two point correlation function and the chord length distribution functions for each 3D reconstructed image. The results are presented in Figs. 8, 9, and 10, for the two point auto-correlation function, pore chord length and mass (solid) chord length distribution function, respectively, for the averaged structures. Similar results have been observed for each bead separately.

In Fig. 8 the two-point auto-correlation functions for the reconstructed domains made by the standard and the hybrid SA method, are compared to the one obtained from averaging all SEM micrographs. The comparison of two-point auto-correlation functions between original and simulated structures made with either method is excellent, as expected, since the objective of the SA algorithm is to match two-point correlation functions between the original and reconstructed images. Note that porosity is already matched by the initial construction of each domain, so in essence the two methods have produced structures that show visual differences, although they have identical zero and first moments of the phase function. Therefore, in order to search for structural differences between the two 3D

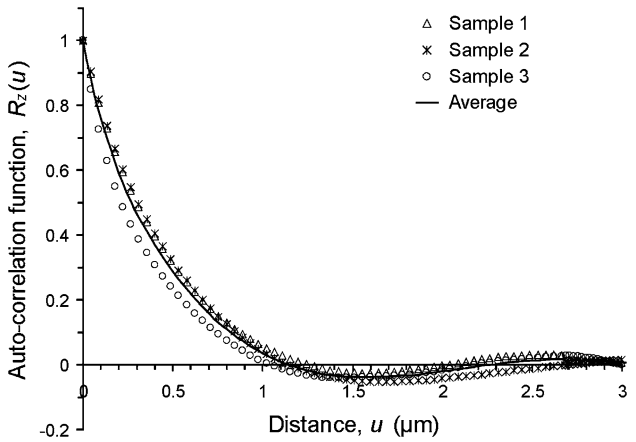

Fig. 4 Two-point auto-correlation functions for the three beads of the zeolite adsorbent

domains, we have calculated chord-length distribution functions, since these properties contain information of higher order moments of the phase function.

In Fig. 9, the cumulative pore chord length distribution functions for the reconstructed domains made by the two methods, are compared to the one obtained by averaging all SEM micrographs. In the same figure we plot the respective pore chord length distribution function for the initial RSP-CS structure used in the hybrid SA method. It is seen that the hybrid method with $T = 10^{-10}$ produces a pore chord length distribution function that is in excellent agreement with that measured in the SEM micrographs. The standard SA method, produces a pore chord length distribution function that under predicts the experimental one, resulting in pore chords that are slightly larger than the ones produced by the hybrid method or measured experimentally (the maximum difference in the whole range is <0.1 μm). Furthermore, the hybrid method with $T = 10^{-8}$ produces a pore chord length distribution function that is located between the hybrid with $T = 10^{-10}$ and the standard SA method, while the pore chord length distribution function of the RSP-CS structure lies above all respective curves showing a sharper a distribution of pore chords.

In Fig. 10, the cumulative mass (solid) chord length distribution functions for the reconstructed domains made by the two methods, are compared to the one obtained by averaging all SEM micrographs. It is seen that the hybrid method with $T = 10^{-10}$ produces a mass chord length distribution function that is still in very good agreement

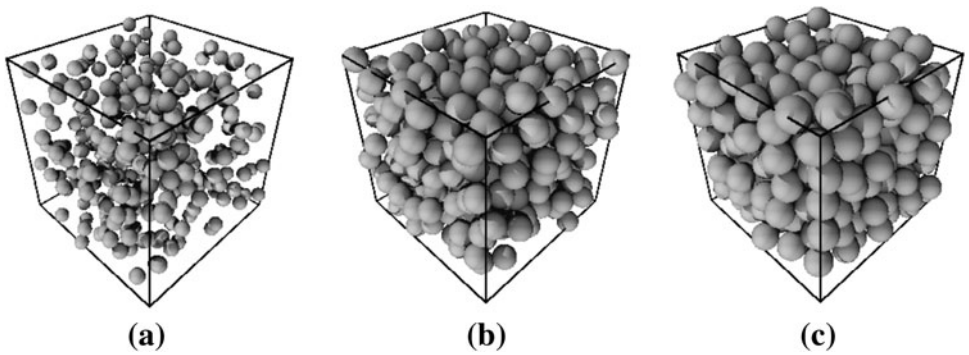

Fig. 5 Snap-shots during the formation of a mono-disperse RSP using the L–S algorithm. The porosity at each stage is, **a** 90 %, **b** 62 % and **c** 40 %

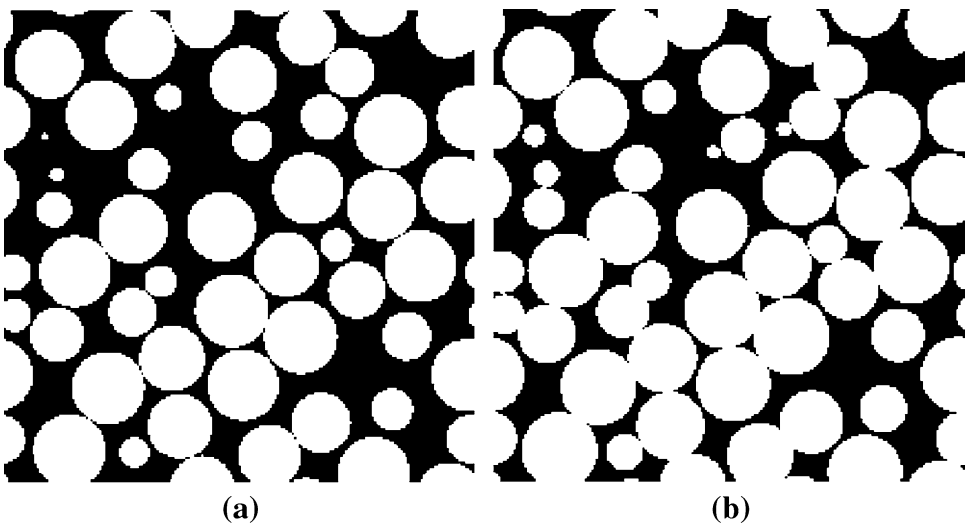

Fig. 6 Two dimensional cuts from digitized structures corresponding to **a** random and **b** consolidated sphere packs with porosities 40 and 32 %, respectively. *Black color* corresponds to void and *white color* to solid phase, respectively

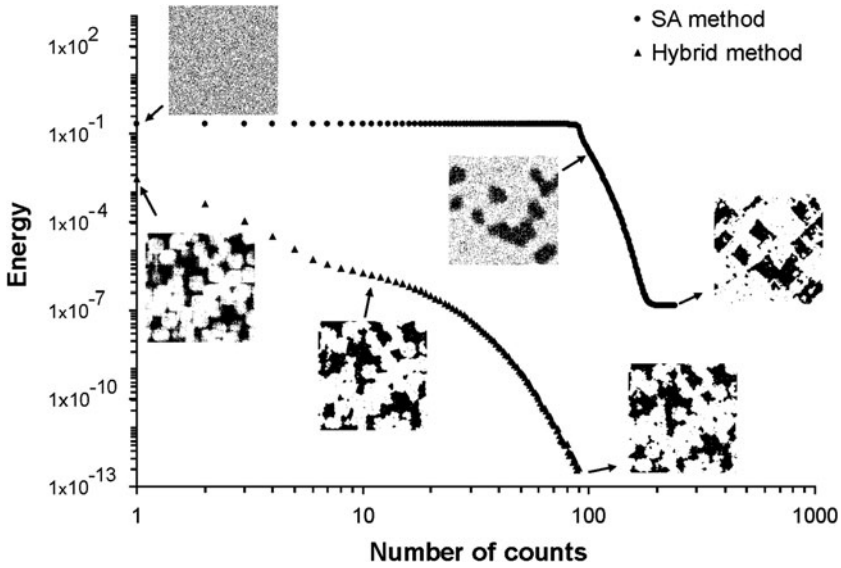

Fig. 7 Energy and structure history (in the form of 2D sections) for 3D structures generated with the standard SA method and the hybrid method with $T = 1\times10^{-10}$

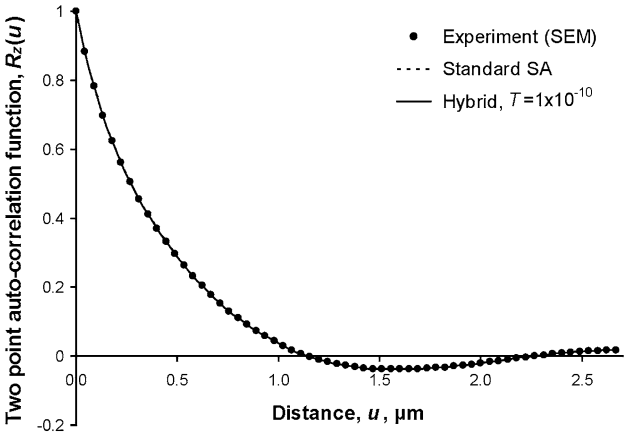

Fig. 8 Comparison of two-point auto-correlation functions between 3D structures made by the SA method and the hybrid method with $T = 1\times10^{-10}$, and with the experimental curve measured on the actual SEM micrographs

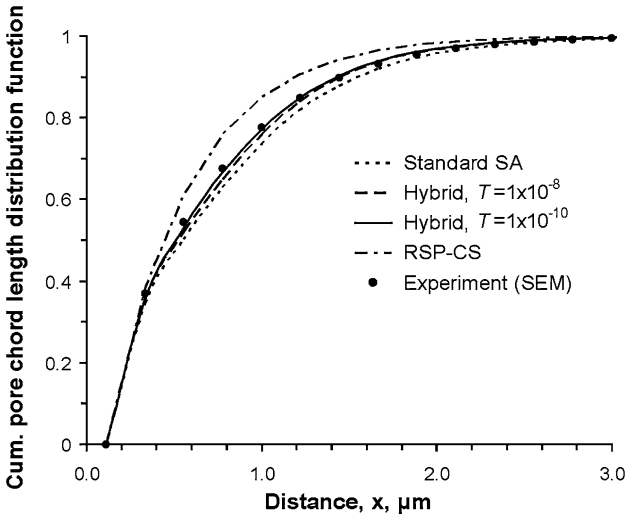

Fig. 9 Pore chord-length distribution functions measured on various simulated 3D structures and on the actual SEM micrographs

with that measured in the SEM micrographs. The standard SA method, on the other hand, produces a mass chord length distribution function that under predicts the experimental one quite significantly, resulting in solid chords that are much larger than the ones produced by the hybrid method or measured experimentally (the maximum difference in the whole range is of the order of 1–1.5 μm). This important difference in mass chord length distribution functions is expected to affect the transport properties of the developed structures as has been observed in related studies (Kainourgiakis et al. 2000; Talukdar et al. 2002b; Politis et al. 2008; Čapek et al. 2009). Furthermore, the hybrid method with $T = 10^{-8}$ produces a mass chord length distribution function that is located again between the hybrid with $T = 10^{-10}$ and the standard SA method, while the mass chord length distribution function of the RSP-CS structure lies above all respective curves showing again a very sharp a distribution of mass solid chords. In essence, mass chord length distribution functions show much more distinct differences among the various structures, compared to pore chord length distribution functions, so we can conclude that this structural property is more sensitive to structural changes than all others examined in this study. The results from Figs. 9 and 10 also justify the use of $T = 10^{-10}$ as a starting temperature in the hybrid method as this selection appears to quantify more accurately the extent of influence of the initial RSP-CS in the final structure.

5 Conclusions

In this first part of the series we have developed and employed advanced experimental and computational

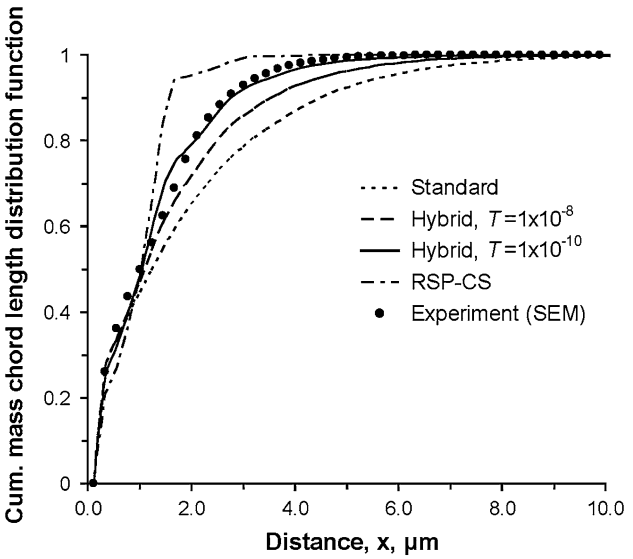

Fig. 10 Mass chord-length distribution functions measured on various simulated 3D structures and on the actual SEM micrographs

methods to characterize the structure of a binderless zeolite adsorbent with improved mass transfer characteristics. More specifically, by using advanced image analysis methods and tools on Back Scattered SEM micrographs, we have been able to extract 2D realistic sections of the porous material and accordingly measure important statistical properties, such as porosity, two point auto-correlation function, pore and mass chord length distribution functions, etc.

Furthermore, we have used standard and hybrid SA methods to stochastically reconstruct in three dimensions the original adsorbent macroporous structure, by matching the first two moments of the phase function, namely porosity and two point auto-correlation function. In the standard SA method we have started from a purely random structure, while in the hybrid SA method we have started from a uniformly consolidated RSP (RSP-CS structure) constructed by the Lubachevsky-Stillinger algorithm.

From the structures developed in the present study using the standard and the hybrid SA method (with $T = 10^{-10}$), respectively, it is found that the latter one preserves, besides the first two moments of the phase function (porosity and two point auto-correlation function), both pore and mass chord length distribution functions of the original structure. Since chord-length distribution functions contain information on higher order moments, we can conclude that the hybrid SA method produces a final 3D structure that preserves significant statistical information of higher order moments, besides that of the first two moments of the phase function. This is because in the hybrid process we have initiated the SA algorithm starting from a structure that contains structural information of the sintered zeolite powder, in the form of a consolidated RSP with the porosity of the final structure. Thanks to the low initial temperature, $T = 10^{-10}$, used in the hybrid process, parts of this initial structural configuration have been preserved and incorporated in the final structure of the zeolite adsorbent agglomerate, as it is probably the case in the actual fabrication process of this material. In the case of the 3D structure made with the standard SA method that starts from a completely random configuration and/or at a high initial temperature that ensures the diminishing of all initial correlations, we can only expect an excellent matching of the first two moments but we have no way of controlling higher order moments. Evidently, diffusion studies will enable us to further evaluate the structures made by each method, as will be explored in Part II of this series.

Acknowledgments We thank Drs. Mark Ackley, Philip Barrett and Neil Stephenson from Praxair, Inc. for stimulating discussions and for providing us with SEM micrographs on the binderless zeolite adsorbent. Financial support from Praxair, Inc. is gratefully acknowledged.

References

Ackley M.W., Leavitt F.W.: Rate-enhanced gas separation. US Patent 6,500,234 (2002)

Ackley M.W., Smolarek J., Leavitt F.W.: Pressure swing adsorption gas separation method, using adsorbents with high intrinsic diffusivity and low pressure ratios. US Patent 6,506,234 (2003)

Ackley M.W., Zhong G.: Medical oxygen concentrator. US Patent 6,511,384 (2003)

Adler, P.M.: Porous Media: Geometry and Transports. Butterworth Heinemann, Stoneham (1992)

Baveye, P.C., Laba, M., Otten, W., Bouckaert, L., Dello Sterpaio, P., Goswami, R.R., Grinev, D., Houston, A., Hu, Y., Liu, J., Mooney, S., Pajor, R., Sleutel, S., Tarquis, A., Wang, W., Wei, Q., Sezgin, M.: Observer-dependent variability of the thresholding step in the quantitative analysis of soil images and X-ray microtomography data. Geoderma **157**(1–2), 51–63 (2010)

Berryman, J.G.: Measurement of spatial correlation functions using image processing techniques. J. Appl. Phys. **57**(7), 2374–2384 (1985)

Bonilla, G., Tsapatsis, M., Vlachos, D.G., Xomeritakis, G.: Fluorescence confocal optical microscopy imaging of the grain boundary structure of zeolite MFI membranes made by secondary (seeded) growth. J. Membr. Sci. **182**, 103–109 (2001)

Breck, D.W.: Zeolite Molecular Sieves: Structure, Chemistry and Use. Krieger Publishing Company, Malabar (1984)

Burganos, V.N., Sotirchos, S.V.: Diffusion in pore networks-effective medium theory and smooth field approximation. AIChE J. **33**(10), 1678–1689 (1987)

Čapek, P., Hejtmánek, V., Brabec, L., Zikánová, A., Kocirík, M.: Stochastic reconstruction of particulate media using simulated annealing: improving pore connectivity. Transp. Porous Media **76**(2), 179–198 (2009)

Čapek, P., Hejtmánek, V., Kolafa, J., Brabec, L.: Transport properties of stochastically reconstructed porous media with improved pore connectivity. Transp. Porous Media **88**(1), 87–106 (2011)

Carniglia, S.C.: Construction of the tortuosity factor from porosimetry. J. Catal. **102**(2), 401–418 (1986)

Chao C.C., Pontonio S.J.: Advanced adsorbent for PSA. US Patent, 6,425,940 (2002)
Collins, T.J.: ImageJ for microscopy. Biotechniques **43**(1 Suppl), 25–30 (2007)
Cule, D., Torquato, S.: Generating random media from limited microstructural information via stochastic optimization. J. Appl. Phys. **86**(6), 3428–3437 (1999)
Do, D.D.: Adsorption Analysis: Equilibria and Kinetics. Imperial College Press, London (1998)
Dukić-Ott, A., Thommes, M., Remon, J.P., Kleinebudde, P., Vervaet, C.: Production of pellets via extrusion–spheronisation without the incorporation of microcrystalline cellulose: a critical review. Eur. J. Pharm. Biopharm. **71**(1), 38–46 (2009)
Echlin, P.: Handbook of Sample Preparation for Scanning Electron Microscopy and X-ray Microanalysis. Springer, New York (2009)
Girish, V., Vijayalakshmi, A.: Affordable image analysis using NIH Image/ImageJ. Indian J. Cancer **41**(1), 47 (2004)
Gonzalez, R.C., Woods, R.E.: Digital Image Processing, 3rd edn. Prentice Hall, Upper Saddle River (2008)
Gonzalez, R.C., Woods, R.E., Eddins, S.L.: Digital Image Processing Using MATLAB, 2nd edn. Gatesmark Publishing, Knoxville (2009)
Hollewand, M.P., Gladden, L.F.: Representation of porous catalysts using random pore networks. Chem. Eng. Sci. **47**(9–11), 2757–2762 (1992)
Jasra, R.V., Tyagi, B., Badheka, Y.M., Choudary, V.N., Bhat, T.S.G.: Effect of clay binder on sorption and catalytic properties of zeolite pellets. Ind. Eng. Chem. Res. **42**(14), 3263–3272 (2003)
Jiao, Y., Stillinger, F.H., Torquato, S.: A superior descriptor of random textures and its predictive capacity. Proc. Natl. Acad. Sci. **106**, 17634 (2009)
Jiao, Y., Stillinger, F.H., Torquato, S.: Geometrical ambiguity of pair statistics II. Heterogeneous media. Phys. Rev. E **82**, 011106 (2010)
Karger, J., Cocirik, M., Zikanova, A.: Molecular transport through assemblages of microporous particles. J. Colloid Interface Sci. **84**(1), 240–249 (1981)
Karger, J., Ruthven, D.M.: Diffusion in Zeolites. Wiley, New York (1992)
Kainourgiakis, M.E., Kikkinides, E.S., Stubos, A.K., Kanellopoulos, N.K.: Simulation of self-diffusion of point-like and finite-size tracers in stochastically reconstructed Vycor porous glasses. J. Chem. Phys. **111**(6), 2735–2743 (1999)
Kainourgiakis, M.E., Kikkinides, E.S., Steriotis, T.A., Stubos, A.K., Tzevelekos, K.P., Kanellopoulos, N.K.: Structural and transport properties of alumina porous membranes from process-based and statistical reconstruction techniques. J. Colloid Interface Sci. **231**(1), 158–167 (2000)
Kainourgiakis, M.E., Kikkinides, E.S., Stubos, A.K.: Diffusion and flow in porous domains constructed using process-based and stochastic techniques. J. Porous Mater. **9**(2), 141–154 (2002)
Kikkinides, E.S., Stoitsas, K.A., Zaspalis, V.T., Burganos, V.N.: Simulation of structural and permeation properties of multi-layer ceramic membranes. J. Membr. Sci. **243**(1–2), 133–141 (2004)
Kirkpatrick, S., Gelatt Jr, C.D., Vecchi, M.P.: Optimization by simulated annealing. Science **220**(4598), 671–680 (1983)
Landini, G.: Auto threshold and auto local threshold. http://www.dentistry.bham.ac.uk/landinig/software/autothreshold/autothreshold.html (2011). Accessed 5 Nov 2012
Leon y Leon, C.A.: New perspectives in mercury porosimetry. Adv. Colloid Interface Sci. **76–77**, 341–372 (1998)
Levitz, P.: Off-lattice reconstruction of porous media: critical evaluation, geometrical confinement and molecular transport. Adv. Colloid Interface Sci. **76–77**, 71–106 (1998)
Levitz, P., Tchoubar, D.: Disordered porous solids—from chord distributions to small angle scattering. J. Phys. I **2**(6), 771–790 (1992)
Lowell, S., Shields, J.E.: Powder Surface Area and Porosity, 3rd edn. Chapman and Hall, London (1991)
Lubachevsky, B.D., Stillinger, F.H.: Geometric properties of random disk packings. J. Stat. Phys. **60**(5–6), 561–583 (1990)
Manay, S., Yezzi, A.: Anti-geometric diffusion for adaptive thresholding and fast segmentation. IEEE Trans. Image Process. **12**(11), 1310–1323 (2003)
Øren, P.E., Bakke, S.: Process based reconstruction of sandstones and prediction of transport properties. Transp. Porous Media **46**(2–3), 311–343 (2002)
Papadopoulos, G.K., Theodorou, D.N., Vasenkov, S., Karger, J.: Mesoscopic simulations of the diffusivity of ethane in beds of NaX zeolite crystals: comparison with pulsed field gradient NMR measurements. J. Chem. Phys. **126**(9), 094702 (2007)
Politis, M.G., Kikkinides, E.S., Kainourgiakis, M.E., Stubos, A.K.: A hybrid process-based and stochastic reconstruction method of porous media. Microporous Mesoporous Mater. **110**(1), 92–99 (2008)
Roberts, A.P.: Statistical reconstruction of three-dimensional porous media from two-dimensional images. Phys. Rev. E **56**(3), 3203–3212 (1997)
Roberts, J.N., Schwartz, L.M.: Grain consolidation and electrical conductivity in porous media. Phys. Rev. B **31**(9), 5990–5997 (1985)
Rouquerol, J., Baron, G.V., Denoyel, R., Giesche, H., Groen, J., Klobes, P., Levitz, P., Neimark, A.V., Rigby, S., Skudas, R., Sing, K., Thommes, M., Unger, K.: The characterization of macroporous solids: an overview of the methodology. Microporous Mesoporous Mater. **154**, 2–6 (2012)
Russ, J.C.: The Image Processing Handbook, 6th edn. CRC, London (2011)
Ruthven, D.M.: Principles of Adsorption and Adsorption Processes. Wiley-Interscience, New York (1984)
Ruthven, D.M.: Past progress and future challenges in adsorption research. Ind. Eng. Chem. Res. **39**(7), 2127–2131 (2000)
Ruthven, D.M., Farooq, S.: Knaebel Pressure Swing Adsorption. Wiley-VCH, New York (1994)
Ruthven, D.M., Xu, Z.: Diffusion of oxygen and nitrogen in 5A zeolite crystals and commercial 5A pellets. Chem. Eng. Sci. **48**(18), 3307–3312 (1993)
Sahimi, M., Gavalas, G.R., Tsotsis, T.T.: Statistical and continuum models of fluid–solid reactions in porous media. Chem. Eng. Sci. **45**(6), 1443–1502 (1990)
Schneider, C.A., Rasband, W.S., Eliceiri, K.W.: NIH image to ImageJ: 25 years of image analysis. Nat. Methods **9**(7), 671–675 (2012)
Sezgin, M., Sankur, B.: Survey over image thresholding techniques and quantitative performance evaluation. J. Electron. Imaging **13**(1), 146–168 (2004)
Shapiro, L.G., Stockman, G.C.: Computer Vision. Prentice Hall, Upper Saddle River (2001)
Sircar, S.: Applications of gas separation by adsorption for the future. Adsorpt. Sci. Technol. **19**(5), 347–366 (2001)
Sircar, S.: Pressure swing adsorption. Ind. Eng. Chem. Res. **41**(6), 1389–1392 (2002)
Talukdar, M.S., Torsaeter, O., Ioannidis, M.A., Howard, J.J.: Stochastic reconstruction, 3D characterization and network modeling of chalk. J. Petrol. Sci. Eng. **35**(1–2), 1–21 (2002a)
Talukdar, M.S., Torsaeter, O., Ioannidis, M.A.: Stochastic reconstruction of particulate media from two-dimensional images. J. Colloid Interface Sci. **248**(2), 419–428 (2002b)
Tarquis, A.M., Heck, R.J., Grau, J.B., Fabregat, J., Sanchez, M.E., Antón, J.M.: Influence of thresholding in mass and entropy

dimension of 3-D soil images. Nonlinear Process Geophys **15**(6), 881–891 (2008)

Todd, R.S., Webley, P.A.: Limitations of the LDF/equimolar counterdiffusion assumption for mass transport within porous adsorbent pellets. Chem. Eng. Sci. **57**(19), 4227–4242 (2002)

Todd, R.S., Webley, P.A.: Macropore diffusion dusty-gas coefficient for pelletised zeolites from breakthrough experiments in the O_2/N_2 system. Chem. Eng. Sci. **60**, 4593–4608 (2005)

Torquato, S.: Random Heterogeneous Materials: Microstructure and Macroscopic Properties. Springer, New York (2002)

Torquato, S., Truskett, T.M., Debenedetti, P.G.: Is random close packing of spheres well defined? Phys. Rev. Lett. **84**(10), 2064–2067 (2000)

Tschumperle, D., Deriche, R.: Vector-valued image regularization with PDEs: a common framework for different applications. IEEE Trans. Pattern Anal. Mach. Intell. **27**(4), 506–517 (2005)

Wankat, P.C.: Intensification of sorption processes. Ind. Eng. Chem. Res. **26**(8), 1579–1585 (1987)

Yang, R.T.: Gas Separation by Adsorption Processes. Butteworth, Boston (1987)

Yang, R.T.: Adsorbents: Fundamentals and Applications. Wiley-Interscience, New York (2003)

Yeong, C.L.Y., Torquato, S.: Reconstructing random media. Phys. Rev. E **57**(1), 495–506 (1998a)

Yeong, C.L.Y., Torquato, S.: Reconstructing random media. II. Three-dimensional media from two-dimensiomal cuts. Phys. Rev. E **58**(1), 224–233 (1998b)

Zhang, L., Seaton, N.A.: Prediction of the effective diffusivity in pore networks close to percolation-threshold. AIChE J. **38**(100), 1816–1824 (1992)